

NUMERICAL SIMULATIONS OF NON-NEWTONIAN JETS

Giovanni Soligo

Complex Fluids and Flows Unit

Okinawa Institute of Science and Technology Graduate University
1919-1 Tancha, Onna-son, Kunigami-gun, Okinawa, 904-0495, Japan
soligo.giovanni@oist.jp

Marco Edoardo Rosti

Complex Fluids and Flows Unit

Okinawa Institute of Science and Technology Graduate University
1919-1 Tancha, Onna-son, Kunigami-gun, Okinawa, 904-0495, Japan
marco.rosti@oist.jp

ABSTRACT

Jets are a type of flow representative of more complex flow configurations commonly found in nature and in industrial applications. Their importance led to a significant progress in the understanding of the dynamics of jet flows via analytic solution of simplified equations, numerical simulations and experiments. Most of these studies however focused on Newtonian fluids, while very few works involved non-Newtonian fluids. These latter fluids are characterized by complex fluid properties, as for instance fluid elasticity or shear-dependent viscosity, which lead to the onset of a richer flowing behavior. Our aim is to advance the current understanding of jets of non-Newtonian fluids through direct numerical simulations of different non-Newtonian fluids at low Reynolds numbers. We observe an earlier transition to a turbulent regime, here intended in a more general meaning as disordered fluid motions. This regime is qualitatively different from Newtonian turbulence; turbulent kinetic energy spectra allow us to provide as well a quantitative characterization of this flowing regime.

INTRODUCTION

The flow of non-Newtonian fluids exhibits very different flowing patterns depending on the flowing conditions; recent experiments (Yamani *et al.*, 2021) showed the onset of substantially different flowing pattern when the Reynolds (ratio of inertial over viscous contributions) and Weissenberg (ratio of the polymer relaxation time over a flow time scale) numbers were changed. The observed flow is the result of the competition of inertial, viscous and elastic contributions, ranging from laminar flow, Newtonian turbulence, elasto-inertial filaments and elasto-inertial turbulence. The onset of disordered fluid motions in non-Newtonian fluids is also observed at a Reynolds number much lower for what observed for Newtonian fluids in the very same flowing configuration. This finding hints at the existence of a different pathway to turbulence; it has been proven that fluid elasticity is indeed a key element in triggering flow instabilities (Joo & Shaqfeh, 1994; Kumar *et al.*, 2021; Walkama *et al.*, 2020; De *et al.*, 2017; Grilli *et al.*, 2013; Joo & Shaqfeh, 1992; Khalid *et al.*, 2021). In this work

we will focus on a relatively unexplored region of the parameter space: the effect of increasing Weissenberg numbers at low Reynolds number will be investigated. We consider three different fluid models: Carreau (shear-thinning), Giesekus (shear-thinning and viscoelastic) and Oldroyd-B (viscoelastic). A reference simulation of a Newtonian fluid completes the database.

We compute the classical jet statistics, namely the center-line velocity and jet thickness; previous works with a FENE-P model (shear-thinning and viscoelastic fluid) showed that these bulk quantities recover the power-law scalings obtained for a Newtonian fluid in laminar (Parvar *et al.*, 2020) and turbulent (Guimarães *et al.*, 2020) planar jets. The universal validity of these scaling laws can be traced back to their derivation: no hypothesis on the fluid model is taken, hence it is expected that they still hold true for non-Newtonian fluids and apply as well to different non-Newtonian fluid models. We then proceed to quantitatively characterize the different flowing patterns observed at the highest value of the Weissenberg number. It is clear that when the fluid is characterized by flow elasticity, a different power-law scaling appears in the energy spectrum of the turbulent kinetic energy.

In the following, the numerical method we use for our simulation and the simulation setup are reported in the first section. We then present the main results from our numerical simulations, starting from a qualitative visualization of the stream-wise velocity field at steady-state, moving then to the bulk statistics and lastly to the turbulent kinetic energy spectrum. In the last section, the main findings are summarized.

COMPUTATIONAL SETUP

To simulate the dynamics of the planar jet we use direct numerical simulations of the Navier-Stokes and continuity equations, respectively equations 1 and 2, coupled with a transport equation for the non-Newtonian extra-stress tensor, equation 3. We use \mathbf{u} as the fluid velocity, t is time, ρ is the fluid density (homogeneous in space and constant in time), η_s and η_p respectively are the solvent and polymeric dynamic viscosity, p is the pressure, $\boldsymbol{\tau}$ is the non-Newtonian extra-stress-tensor, λ is the polymer relaxation time scale and α is the mo-

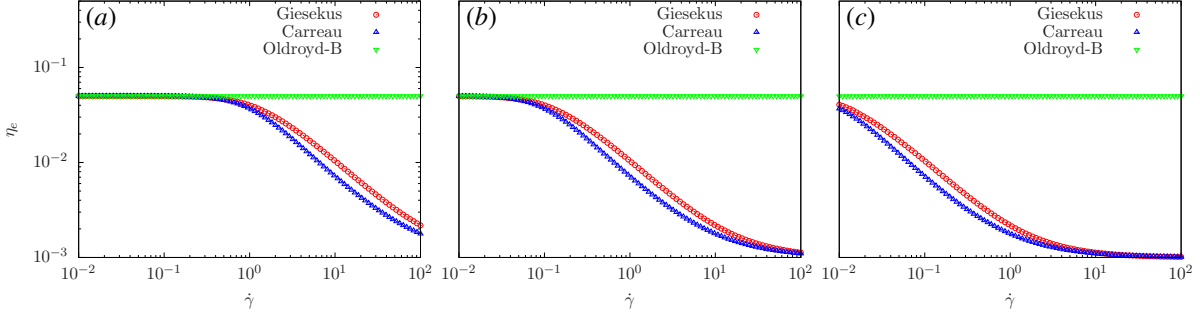


Figure 1. Rheology of the different fluid models for increasing Weissenberg numbers; from left to right panel (a) $Wi = 1$, panel (b) $Wi = 10$ and panel (c) $Wi = 100$.

bility parameter of the Giesekus fluid (equal to zero for the Oldroyd-B fluid model).

$$\rho \left(\frac{\partial \mathbf{u}}{\partial t} + \mathbf{u} \cdot \nabla \mathbf{u} \right) = -\nabla p + \nabla \left[\eta_s \left(\nabla \mathbf{u} + \nabla \mathbf{u}^T \right) \right] + \nabla \cdot \boldsymbol{\tau} \quad (1)$$

$$\nabla \cdot \mathbf{u} = 0 \quad (2)$$

$$\boldsymbol{\tau} + \lambda \overset{\nabla}{\boldsymbol{\tau}} + \frac{\alpha \lambda}{\eta_p} \boldsymbol{\tau} \cdot \boldsymbol{\tau} = \eta_p \left(\nabla \mathbf{u} + \nabla \mathbf{u}^T \right) \quad (3)$$

The upper-convected derivative, $\overset{\nabla}{\boldsymbol{\tau}}$, is defined as follows.

$$\overset{\nabla}{\boldsymbol{\tau}} = \frac{\partial \boldsymbol{\tau}}{\partial t} + \mathbf{u} \cdot \nabla \boldsymbol{\tau} - \left(\nabla \mathbf{u}^T \cdot \boldsymbol{\tau} + \boldsymbol{\tau} \cdot \nabla \mathbf{u} \right) \quad (4)$$

We solve the extra-stress transport equation only for the Giesekus and Oldroyd-B fluid models. The Carreau fluid, on the other hand, does not include any polymer-induced extra-stresses; the solvent viscosity η_s however depends on the local shear rate, $\dot{\gamma}$, as reported in equation 5.

$$\eta_s = \eta_\infty + (\eta_0 - \eta_\infty) \left[1 + (\lambda \dot{\gamma})^2 \right]^{\frac{n-1}{2}} \quad (5)$$

Here the viscosities at zero shear rate and at infinite shear rate are respectively η_0 and η_∞ . For the Carreau fluid the parameter λ is the fluid consistency index and carries no information on flow elasticity. However, in the sake of simplicity, we will still refer to the ratio of the fluid consistency index over a flow time-scale as the Weissenberg number. Lastly, the power-law index, n , defines whether the fluid is shear-thickening ($n > 1$) or shear-thinning ($n < 1$). In this work we consider a shear-thinning fluid, with power-law index $n = 0.2$.

A common issue that arises when solving the transport equation for the extra-stress tensor, equation 3, is the high-Weissenberg number problem (Keunings, 1986), which leads to the unphysical loss of positive-definiteness of the conformation tensor. This issue occurs at large Weissenberg numbers and manifests as disturbances amplifying over time in the conformation tensor (Dupret & Marchal, 1986; Min *et al.*, 2001; Sureshkumar & Beris, 1995). Different solutions have been suggested to address the high-Weissenberg number problem:

artificial diffusivity can be added to the equation to damp the disturbances (Alves *et al.*, 2000; Mompean & Deville, 1997). This however reduces the accuracy of the calculations (Dubief *et al.*, 2005). We opt instead for the matrix-logarithm formulation of the transport equation of the non-Newtonian extra-stress (Fattal & Kupferman, 2004; Hulsen *et al.*, 2005); this methodology, while being computationally expensive, as it requires solving an eigenvalues/eigenvectors problem on the conformation tensor, is however exact.

The equations are discretized on a staggered, uniform, Cartesian grid; velocity data is stored at the cell faces, while all other variables at the cell center. A second-order finite difference scheme is used to approximate spatial derivative; for the advection term of the extra-stress transport equation a fifth-order WENO scheme is instead adopted (Shu, 2009; Sugiyama *et al.*, 2011). The equations are discretized in time with a second-order, explicit Adams-Bashforth scheme. Time advancement is performed via a fractional-step method (Kim & Moin, 1985), coupled with a fast pressure solver (Dodd & Ferrante, 2014) for the Poisson equation for the pressure.

All simulations have been performed using the in-house code *Fujin*, which has been extensively used and validated in the past (Brizzolara *et al.*, 2021; Mazzino & Rosti, 2021; Olivieri *et al.*, 2020; Rosti *et al.*, 2021a,b; Rosti & Brandt, 2020; Rosti *et al.*, 2019, 2020). Additional validation tests are available at <https://groups.oist.jp/cffu/code>.

To investigate non-Newtonian effects on the dynamic of a planar jet we perform numerical simulations of three different non-Newtonian fluid models, namely Carreau, Giesekus and Oldroyd-B. This way the effects of shear-thinning, fluid elasticity and of their combined effect can be sorted out. The rheology of the different fluid models is reported in figure 1 for all the simulated Weissenberg numbers. The Reynolds number, computed using the inlet velocity v_{in} , the half-height of the slit through which the fluid is issued h and the zero-shear viscosity, is $Re = 20$. An additional, reference simulation of a Newtonian fluid is also performed; at this value of the Reynolds number we observe a laminar flowing regime for this latter case. We perform two-dimensional simulation at low Weissenberg number in a domain of size $160h \times 240h$ (stream-wise \times jet-normal directions) discretized with 1536×2304 grid points. The simulations at the highest Weissenberg number are performed on a three-dimensional domain of size $160h \times 240h \times 13.3h$ (stream-wise \times jet-normal \times span-wise directions), discretized using $1536 \times 2304 \times 128$ grid points. In the following the x coordinate denotes the span-wise direction, y the stream-wise direction and z the jet-normal direction.

The jet is issued from a slit of height $2h$ on the left side of the domain into a pool of the same fluid at rest. No-slip and no-flux boundary conditions are applied at the left boundary, except at the slit through which the fluid is issued. Free-slip

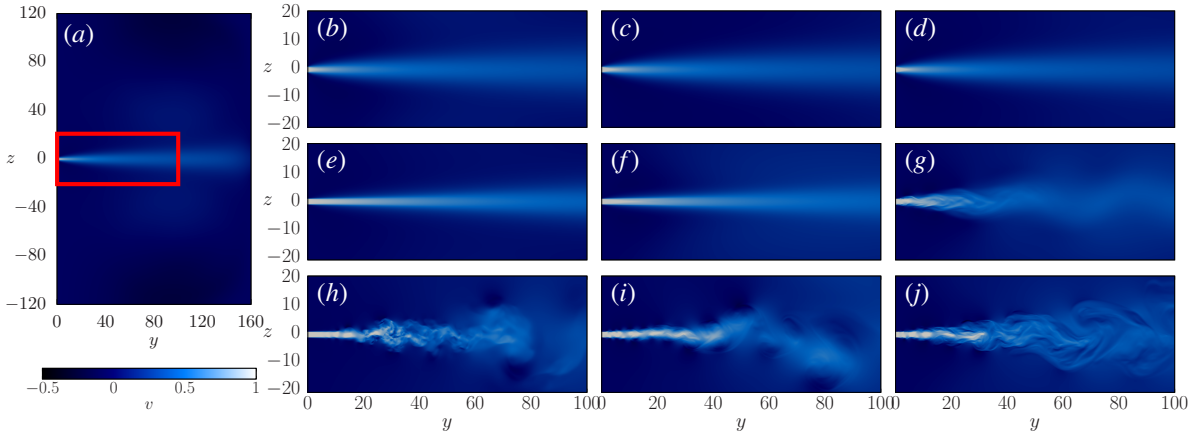


Figure 2. Stream-wise fluid velocity v at steady-state conditions. The Newtonian reference case is reported in panel (a) on the full domain; the red box highlights the region of the domain that is shown in the panels (b)-(j). Each column refers to a different fluid model, Carreau in panels (b), (e), (h), Giesekus in panels (c), (f), (i) and Oldroyd-B in panels (d), (g), (j). Each row correspond to a different Weissenberg number: from top to bottom $Wi = 1$ in panels (b)-(d), $Wi = 10$ in panels (e)-(g) and $Wi = 100$ in panels (h)-(j).

boundary conditions are imposed at the top and bottom boundaries. A non-reflective boundary condition (Orlanski, 1976) is enforced at the outlet section, right boundary.

RESULTS

The stream-wise velocity for all simulated cases is reported in figure 2. It can be immediately noticed the effect of the Weissenberg number, increasing from the top to the bottom row, and of the fluid model. Only a portion of the domain is reported in panels (b)-(j), bounded by the red box in panel (a). At low Weissenberg number, top row, the non-Newtonian contribution is weak and all cases exhibit a laminar flowing regime. As will be quantitatively shown in the following, no appreciable difference is seen among the various cases. As the Weissenberg number is increased to $Wi = 10$, middle row, the onset of an instability can be seen for the Oldroyd-B model; at this intermediate Weissenberg number fluid elasticity starts playing a dominant role over viscous contributions. For the Carreau fluid model, the effect of shear-thinning is still too weak to trigger any flow instability; similarly for the Giesekus fluid model. The laminar flowing regime displayed by the Giesekus fluid at this value of the Weissenberg number hints that while viscoelasticity promotes the transition to a turbulent-like regime, shear-thinning, competing against fluid elasticity, hinders or at least delays such transition. As we move to the highest Weissenberg number, $Wi = 100$, we can immediately notice a striking difference among the three non-Newtonian fluid models: while all cases are characterized by disordered, turbulent-like fluid motions, the flowing pattern is very different. Indeed, the mechanisms generating these disordered fluid motions are different: for the Carreau fluid (shear-thinning) it is the competition between inertial and viscous contributions, for the Giesekus fluid (shear-thinning and viscoelastic) by the competing effect of inertial, elastic and viscous contributions, while for the Oldroyd-B (viscoelastic) by the competition of fluid elasticity and viscous terms.

The flow visualization, figure 2, clearly shows important differences among the various fluid models, in particular at higher Weissenberg numbers, where the contribution from the non-Newtonian component is stronger. The Carreau fluid, being a shear-thinning fluid, exhibits turbulence motions more similar to classical, Newtonian turbulence as the local viscosity is decreased. The Giesekus fluid has a very similar rheo-

logical curve to the Carreau fluid, however fluid elasticity plays an important role as well. The lower value of the local viscosity leads to an increase of the local Reynolds number, thus justifying the transition to a turbulent-like regime. On the contrary, the viscosity of the Oldroyd-B fluid is constant, thus the disordered fluid motions we observe can be traced back to the fluid elasticity alone. Despite the very different flowing regime and rheological curves of the various fluid models, it is interesting to note that the bulk statistics still obey the power-law scalings computed for planar jets of a Newtonian fluid in both laminar and turbulent regime. This result may be unexpected at first, however no assumption on the actual fluid model is made in the derivation of these scaling laws (Parvar *et al.*, 2020; Guimarães *et al.*, 2020). Figures 3 and 4 report respectively the decay of the centerline velocity and the increase in the jet thickness along the stream-wise direction. The jet thickness, $\delta_{0.5}$, is here defined as the distance from the jet centerline at which the time- and space-averaged velocity equals half the centerline velocity at the same stream-wise location. At the lowest Weissenberg number, $Wi = 1$, non-Newtonian effects are weak and viscous contributions dominate the flow. The qualitative visualization shows no difference between the Newtonian reference case and the three non-Newtonian fluid models. This finding is confirmed also by the bulk statistics: the centerline velocity, figure 3(a), and the jet thickness, figure 4, fall on top of each other for all cases, following the laminar power-law scalings, $v_c \propto y^{-1/3}$ and $\delta_{0.5} \propto y^{2/3}$.

As the Weissenberg number is increased to $Wi = 10$ (intermediate Weissenberg number), effects from the non-Newtonian component, namely shear-thinning, fluid elasticity or both combined, become stronger. For the Carreau fluid the reduction in the local viscosity is not sufficient to destabilize the flow and transition to a turbulent-like regime: further away from the inlet the laminar scalings are recovered for both the centerline velocity and the jet thickness. It is interesting to note that memory of the inlet conditions is carried over a longer stream-wise distance: while for the Newtonian case the laminar solution is recovered from about $y = 5$, for the non-Newtonian cases transition towards the power-law scalings occurs further away once the non-Newtonian contribution becomes dominant. Similarly, the Giesekus fluid follows the laminar power-law scalings for both the centerline velocity and the jet thickness at this intermediate Weissenberg number. On the contrary, the Oldroyd-B fluid shows an initial turbulent-

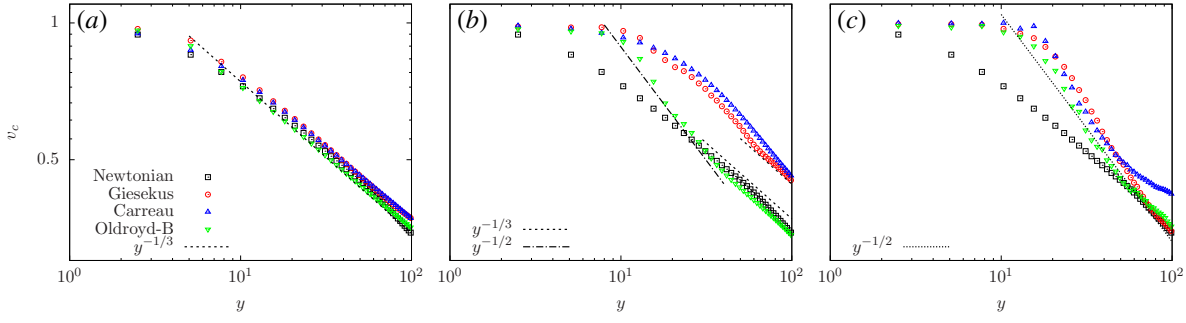


Figure 3. Centerline velocity for different Weissenberg numbers, panel (a) $Wi = 1$, panel (b) $Wi = 10$ and panel (c) $Wi = 100$. The analytic power-law scaling are reported with a dashed line (laminar scaling, $v_c \propto y^{-1/3}$) and dash-dotted line (turbulent scaling, $v_c \propto y^{-1/2}$).

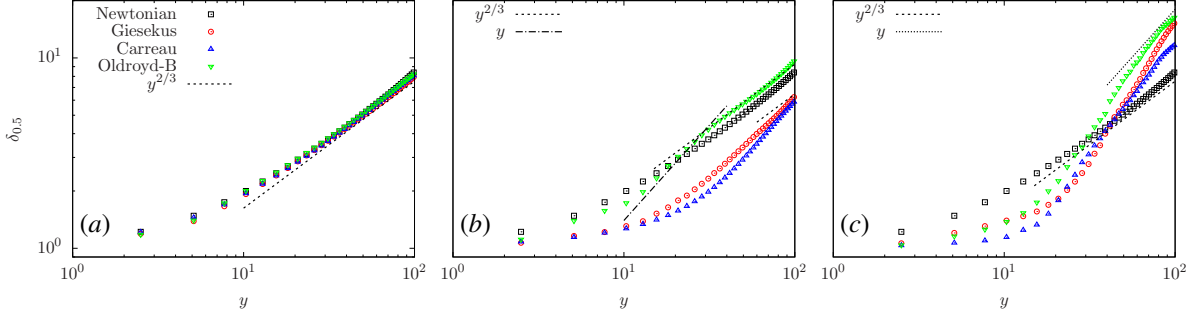


Figure 4. Jet thickness for different Weissenberg numbers, panel (a) $Wi = 1$, panel (b) $Wi = 10$ and panel (c) $Wi = 100$. The analytic power-law scaling are reported with a dashed line (laminar scaling, $\delta_{0.5} \propto y^{2/3}$) and dash-dotted line (turbulent scaling, $\delta_{0.5} \propto y$).

like flowing regime closer to the inlet, at $10 < y < 40$, followed by a transition towards a laminar scaling beyond $y = 40$. We computed the Deborah number (ratio of the polymer time scale over a local flow time scale, not shown here) using local quantities: the relaxation time of the polymer, λ , and the local flow time scale $\delta_{0.5}/v_c$. The value of the Deborah number is larger than one up to $y = 40$ and then reduces below one beyond this stream-wise location. This indicates that fluid elasticity is predominant up to roughly $y = 40$ (Deborah number larger than one), then viscous contributions become dominant (Deborah number lower than one) and the flow transitions to a laminar-like regime. These different flowing regimes can also be seen in figure 2(g) where the initial disordered fluid motions are dissipated roughly beyond $y = 40$. This result hints at a competition between shear-thinning and fluid elasticity: at the intermediate Weissenberg number, the Oldroyd-B fluid shows an initial transition towards a turbulent regime, while the Giesekus fluid model does not exhibit any flow instability, suggesting that shear-thinning hinders, or at least delays, the transition to a turbulent-like regime.

Lastly, at the highest Weissenberg number all fluid models exhibit a turbulent-like flowing regime. Although the flowing pattern is qualitatively different among the various fluid models, the same power-law scalings for Newtonian turbulent planar jets is recovered for all fluid models. For the Carreau fluid the local viscosity is lower, as indicated in figure 1(c), thus reducing the contribution of the viscous terms and leading to a higher local Reynolds number. Transition to turbulence is then promoted by the predominance of inertial over viscous terms. Further away from the inlet the shear rate is lower, thus leading to a higher value of the local viscosity; turbulent motions are then dissipated. The Giesekus fluid, having a similar rheological curve to the Carreau fluid, experiences a similar reduction in the value of the local viscosity. In addition, the polymers within the fluid are more stretched, as indicated by the conformation tensor. The combined effect of these two factors

destabilizes the flow and originates a turbulent-like flow. Fluid elasticity is instead the only factor promoting flow destabilization in the Oldroyd-B fluid: the stretching and retracting of the polymers induce disordered fluid motions; despite the pathway to this turbulent-like regime being very different from that of Newtonian turbulence, we observe that the centerline velocity and jet thickness still obey the computed power-law scalings for a Newtonian turbulent planar jet.

We then proceed to quantitatively characterize the different flowing patterns we observed at the highest Weissenberg number. We compute the turbulent kinetic energy spectra for the three fluid models at $Wi = 100$; we record velocity data over time at a fixed stream-wise location, $y = 40$, at the jet centerline and compute the spectra in time. Several authors have observed scaling exponents within the inertial range different from that characteristic of the Newtonian turbulent energy cascade, $\chi = -5/3$ (Balkovsky *et al.*, 2001; Fouxon & Lebedev, 2003; Perlekar *et al.*, 2010; Vonlanthen & Monkewitz, 2013; Zhang *et al.*, 2021). While most of these studies agree on a steeper decay law, there is yet no general consensus on the actual value of the scaling exponent, with theoretical predictions by Balkovsky *et al.* (2001) and Fouxon & Lebedev (2003) finding a value for the exponent $\chi \leq -3$ and experimental measurements by Vonlanthen & Monkewitz (2013) reporting a power-law exponent $\chi = -3$. Figure 5 reports the computed turbulent kinetic energy power spectra for all fluid models at the highest Weissenberg number. The Carreau fluid follows a clear $\chi = -5/3$ power law exponent in the inertial range: the turbulent fluid motion observed is indeed akin to classical Newtonian turbulence, being originated by the predominance of inertial over viscous contributions. The Giesekus and Oldroyd-B fluids instead show a marked $\chi = -3$ power law exponent; both fluid models are characterized by fluid elasticity, and shear-thinning for the Giesekus fluid alone. The measured scaling exponent well agrees with the measurements by Vonlanthen & Monkewitz (2013); it is also interesting to note

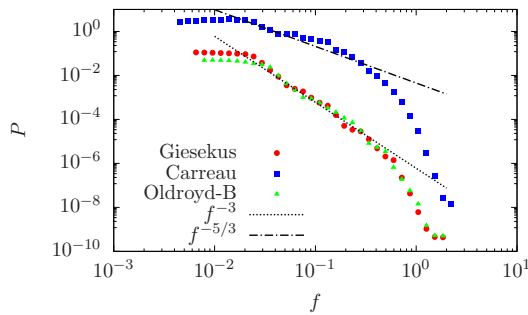


Figure 5. Turbulent kinetic energy spectra for the three non-Newtonian fluid models at the highest Weissenberg number, $Wi = 100$. Velocity data are collected over time at the jet centerline at $y = 40$. The data for the Carreau fluid is shifted upwards for improved readability.

that despite the local Reynolds number for the Giesekus fluid is large enough for Newtonian turbulence to be generated, we do not observe a $\chi = -5/3$ scaling in the inertial regime, suggesting that the contribution from fluid elasticity prevails over inertial terms.

CONCLUSIONS

We performed numerical simulations of a planar jet at low Reynolds number using different non-Newtonian fluid models characterized by shear-thinning (Carreau), shear-thinning and viscoelasticity (Giesekus) and viscoelasticity alone (Oldroyd-B). We changed the strength of the non-Newtonian contribution via a dimensionless parameter, the Weissenberg number, defined as the ratio of the polymer relaxation time scale (or the fluid consistency index for the shear-thinning Carreau fluid) over the flow time scale. For increasing values of the Weissenberg number we observe that the flow, initially laminar, transitions to a turbulent-like regime. Flow visualization at steady-state conditions shows that the flowing regimes are substantially different among the various fluid models: for the Carreau fluid turbulence is a result of the competition between inertial and viscous terms, for the Giesekus fluid it is among inertial, elastic and viscous terms, while for the Oldroyd-B fluid it is between elastic and viscous terms. This difference is also clear from the power spectra of the turbulent kinetic energy: the Carreau fluid shows the same inertial-range power law exponent $\chi = -5/3$ as Newtonian turbulence, while the Giesekus and Oldroyd-B fluid models follow a $\chi = -3$ power law decay in agreement with Vonlanthen & Monkewitz (2013). It is interesting to note that despite the different flowing regimes and energy spectra observed, the bulk statistics, namely the centerline velocity and jet thickness, still follow the same power-law scalings derived for Newtonian planar jets in both laminar and turbulent conditions. While this may seem a surprising result at first, it is not so unexpected as no assumption on the actual fluid model is taken in the derivation of these scalings. Indeed at low Weissenberg numbers we observe a laminar-like flow, which turns unstable and transitions to turbulence as the Weissenberg number is increased; here the key parameter determining the transition to a turbulent-

like flowing regime is the Weissenberg number, rather than the Reynolds number, as it quantifies the strength of non-Newtonian effects. We note that viscoelasticity alone seems to promote the transition to a turbulent-like regime, with the Oldroyd-B fluid showing turbulent motion already at the intermediate Weissenberg number, while shear-thinning seems to hinder the action of fluid elasticity, as suggested by the laminar flowing regime of the Giesekus fluid at the same Weissenberg number.

REFERENCES

- Alves, MA, Pinho, FT & Oliveira, PJ 2000 Effect of a high-resolution differencing scheme on finite-volume predictions of viscoelastic flows. *J. Non-Newtonian Fluid Mech.* **93** (2-3), 287–314.
- Balkovsky, E, Fouxon, A & Lebedev, V 2001 Turbulence of polymer solutions. *Physical Review E* **64** (5), 056301.
- Brizzolara, Stefano, Rosti, Marco Edoardo, Olivieri, Stefano, Brandt, Luca, Holzner, Markus & Mazzino, Andrea 2021 Fiber tracking velocimetry for two-point statistics of turbulence. *Phys. Rev. X* **11** (3), 031060.
- De, Shauvik, Kuipers, JAM, Peters, EAJF & Padding, JT 2017 Viscoelastic flow simulations in random porous media. *J. Non-Newtonian Fluid Mech.* **248**, 50–61.
- Dodd, Michael S & Ferrante, Antonino 2014 A fast pressure-correction method for incompressible two-fluid flows. *J. Computat. Phys.* **273**, 416–434.
- Dubief, Yves, Terrapon, Vincent E, White, Christopher M, Shaqfeh, Eric SG, Moin, Parviz & Lele, Sanjiva K 2005 New answers on the interaction between polymers and vortices in turbulent flows. *Flow Turbul. Combust.* **74** (4), 311–329.
- Dupret, François & Marchal, JM 1986 Loss of evolution in the flow of viscoelastic fluids. *J. Non-Newtonian Fluid Mech.* **20**, 143–171.
- Fattal, Raanan & Kupferman, Raz 2004 Constitutive laws for the matrix-logarithm of the conformation tensor. *J. Non-Newtonian Fluid Mech.* **123** (2-3), 281–285.
- Fouxon, A & Lebedev, V 2003 Spectra of turbulence in dilute polymer solutions. *Physics of Fluids* **15** (7), 2060–2072.
- Grilli, Muzio, Vázquez-Quesada, Adolfo & Ellero, Marco 2013 Transition to turbulence and mixing in a viscoelastic fluid flowing inside a channel with a periodic array of cylindrical obstacles. *Phys. Rev. Lett.* **110** (17), 174501.
- Guimarães, Mateus C, Pimentel, Nuno, Pinho, Fernando T & da Silva, Carlos B 2020 Direct numerical simulations of turbulent viscoelastic jets. *J. Fluid Mech.* **899**.
- Hulslen, Martien A, Fattal, Raanan & Kupferman, Raz 2005 Flow of viscoelastic fluids past a cylinder at high weissenberg number: stabilized simulations using matrix logarithms. *J. Non-Newtonian Fluid Mech.* **127** (1), 27–39.
- Joo, Yong Lak & Shaqfeh, Eric SG 1992 A purely elastic instability in dean and taylor–dean flow. *Phys. Fluids* **4** (3), 524–543.
- Joo, Yong Lak & Shaqfeh, Eric SG 1994 Observations of purely elastic instabilities in the taylor–dean flow of a boger fluid. *J. Fluid Mech.* **262**, 27–73.
- Keunings, Roland 1986 On the high weissenberg number problem. *J. Non-Newtonian Fluid Mech.* **20**, 209–226.
- Khalid, Mohammad, Shankar, V & Subramanian, Ganesh 2021 Continuous pathway between the elasto-inertial and elastic turbulent states in viscoelastic channel flow. *Phys. Rev. Lett.* **127** (13), 134502.
- Kim, John & Moin, Parviz 1985 Application of a fractional-

- step method to incompressible navier-stokes equations. *J. Computat. Phys.* **59** (2), 308–323.
- Kumar, Manish, Aramideh, Soroush, Browne, Christopher A, Datta, Sujit S & Ardekani, Arezoo M 2021 Numerical investigation of multistability in the unstable flow of a polymer solution through porous media. *Phys. Rev. Fluids* **6** (3), 033304.
- Mazzino, Andrea & Rosti, Marco Edoardo 2021 Unraveling the secrets of turbulence in a fluid puff. *Phys. Rev. Lett.* **127** (9), 094501.
- Min, Taegee, Yoo, Jung Yul & Choi, Haecheon 2001 Effect of spatial discretization schemes on numerical solutions of viscoelastic fluid flows. *J. Non-Newtonian Fluid Mech.* **100** (1-3), 27–47.
- Mompean, Gilmar & Deville, Michel 1997 Unsteady finite volume simulation of oldroyd-b fluid through a three-dimensional planar contraction. *J. Non-Newtonian Fluid Mech.* **72** (2-3), 253–279.
- Olivieri, Stefano, Brandt, Luca, Rosti, Marco E & Mazzino, Andrea 2020 Dispersed fibers change the classical energy budget of turbulence via nonlocal transfer. *Phys. Rev. Lett.* **125** (11), 114501.
- Orlanski, I. 1976 A simple boundary condition for unbounded hyperbolic flows. *J. Comput. Phys.* **21** (3), 251–269.
- Parvar, S, da Silva, CB & Pinho, FT 2020 Local similarity solution for steady laminar planar jet flow of viscoelastic fene-p fluids. *J. Non-Newtonian Fluid Mech.* **279**, 104265.
- Perlekar, Prasad, Mitra, Dhruvadiya & Pandit, Rahul 2010 Direct numerical simulations of statistically steady, homogeneous, isotropic fluid turbulence with polymer additives. *Physical Review E* **82** (6), 066313.
- Rosti, M.E., Ge, Z., Jain, S.S., Dodd, M.S. & Brandt, L. 2019 Droplets in homogeneous shear turbulence. *J. Fluid Mech.* **876**, 962–984.
- Rosti, ME, Olivieri, S, Cavaiola, M, Seminara, A & Mazzino, A 2020 Fluid dynamics of covid-19 airborne infection suggests urgent data for a scientific design of social distancing. *Scientific reports* **10** (1), 1–9.
- Rosti, Marco Edoardo & Brandt, Luca 2020 Increase of turbulent drag by polymers in particle suspensions. *Phys. Rev. Fluids* **5** (4), 041301.
- Rosti, Marco E, Cavaiola, Mattia, Olivieri, Stefano, Seminara, Agnese & Mazzino, Andrea 2021a Turbulence role in the fate of virus-containing droplets in violent expiratory events. *Phys. Rev. Res.* **3** (1), 013091.
- Rosti, Marco E, Perlekar, Prasad & Mitra, Dhruvadiya 2021b Large is different: non-monotonic behaviour of elastic range scaling in polymeric turbulence at large reynolds and Deborah numbers. *arXiv preprint arXiv:2111.11224*.
- Shu, Chi-Wang 2009 High order weighted essentially nonoscillatory schemes for convection dominated problems. *SIAM review* **51** (1), 82–126.
- Sugiyama, Kazuyasu, Ii, Satoshi, Takeuchi, Shintaro, Takagi, Shu & Matsumoto, Yoichiro 2011 A full eulerian finite difference approach for solving fluid–structure coupling problems. *J. Computat. Phys.* **230** (3), 596–627.
- Sureshkumar, R & Beris, Antony N 1995 Effect of artificial stress diffusivity on the stability of numerical calculations and the flow dynamics of time-dependent viscoelastic flows. *J. Non-Newtonian Fluid Mech.* **60** (1), 53–80.
- Vonlanthen, Richard & Monkewitz, Peter A 2013 Grid turbulence in dilute polymer solutions: Peo in water. *Journal of Fluid Mechanics* **730**, 76–98.
- Walkama, Derek M, Waisbord, Nicolas & Guasto, Jeffrey S 2020 Disorder suppresses chaos in viscoelastic flows. *Phys. Rev. Lett.* **124** (16), 164501.
- Yamani, Sami, Keshavarz, Bavand, Raj, Yashasvi, Zaki, Tamer A, McKinley, Gareth H & Bischofberger, Irmgard 2021 Spectral universality of elastoinertial turbulence. *Phys. Rev. Lett.* **127** (7), 074501.
- Zhang, Yi-Bao, Bodenschatz, Eberhard, Xu, Haitao & Xi, Heng-Dong 2021 Experimental observation of the elastic range scaling in turbulent flow with polymer additives. *Science Advances* **7** (14), eabd3525.